The Journal of Chemical Physics

Analytical nuclear gradients for electron-attached and electron-detached states for the second-order algebraic diagrammatic construction scheme combined with frozen-density embedding

Cite as: J. Chem. Phys. **152**, 174109 (2020); https://doi.org/10.1063/5.0002851
Submitted: 28 January 2020 . Accepted: 12 April 2020 . Published Online: 06 May 2020

Jing Liu, Christof Hättig, and Sebastian Höfener

View Online Export Citation CrossMark

ARTICLES YOU MAY BE INTERESTED IN

A basis-set error correction based on density-functional theory for strongly correlated molecular systems
The Journal of Chemical Physics **152**, 174104 (2020); https://doi.org/10.1063/5.0002892

Equation of motion coupled-cluster cumulant approach for intrinsic losses in x-ray spectra
The Journal of Chemical Physics **152**, 174113 (2020); https://doi.org/10.1063/5.0004865

e^T 1.0: An open source electronic structure program with emphasis on coupled cluster and multilevel methods
The Journal of Chemical Physics **152**, 184103 (2020); https://doi.org/10.1063/5.0004713

Lock-in Amplifiers up to 600 MHz
Watch



© 2020 Author(s).

The Journal of Chemical Physics ARTICLE scitation.org/journal/jcp

Analytical nuclear gradients for electron-attached and electron-detached states for the second-order algebraic diagrammatic construction scheme combined with frozen-density embedding

Cite as: J. Chem. Phys. 152, 174109 (2020); doi: 10.1063/5.0002851
Submitted: 28 January 2020 • Accepted: 12 April 2020 •
Published Online: 6 May 2020

View Online Export Citation CrossMark

Jing Liu,[1] Christof Hättig,[2] and Sebastian Höfener[1,a)]

AFFILIATIONS

[1] Institute of Physical Chemistry, Karlsruhe Institute of Technology (KIT), P.O. Box 6980, D-76049 Karlsruhe, Germany
[2] Lehrstuhl für Theoretische Chemie, Ruhr-Universität Bochum, D-44780 Bochum, Germany

[a)] **Author to whom correspondence should be addressed:** hoefener@kit.edu

ABSTRACT

In the present work, we report the derivation and implementation of vertical ionization potentials (IPs) and electron affinities (EAs) for embedded wavefunction methods as well as the corresponding analytical nuclear gradients. Vertical transitions have been implemented for CIS(D_∞), the second-order algebraic diagrammatic construction [ADC(2)] scheme, and the second-order approximate coupled-cluster singles and doubles method. For all methods, density fitting is applied to facilitate reduced memory and disk storage requirements. Analytical nuclear gradients have been derived and implemented for CIS(D_∞) and ADC(2) both with and without frozen-density embedding (FDE). The objective of the reported method is to study the properties of organic semiconductors in which charge is transported along molecular stacks in molecular crystals. The accuracy of the implemented methods is, therefore, assessed using stacked dimers of small model systems. Albeit second-order methods can yield noticeable errors with respect to reference methods in terms of absolute IP and EA values, they show a significantly improved accuracy for the shift of the IP and EA values at different intermolecular distances relative to the monomers. Besides reducing the computational costs, the FDE ansatz introduces furthermore a significant conceptual difference as it enables control over which subsystem is ionized, allowing for the calculation of transfer integrals for the interacting (embedded) systems. The new implementation is finally applied to tetraazaperopyrenes, used as organic semiconductors, to study charge-localization and long-range polarization in particular.

Published under license by AIP Publishing. https://doi.org/10.1063/5.0002851

I. INTRODUCTION

The industrial production of semiconductors has been dominated by inorganic materials for decades. However, the development of semiconductors based on organic materials, especially π-conjugated systems, has been rapidly promoted due to their improved properties, among which are the reduced manufacturing cost and structural flexibility.[1–5]

Polycyclic aromatic compounds are particularly promising and have been employed in various applications. Among them are the tetraazaperopyrenes (TAPPs), which have received some attention in recent years. Combining the TAPP core with electron-withdrawing groups, such as halogen atoms or fluorinated alkyl groups, leads to tuned properties by changing the lowest unoccupied molecular orbital (LUMO) of the π conjugated system.[6–9] This change in the LUMO alters the electron transport behavior by either promoting or hindering electronic excitations of the molecule. In organic semiconductors, electrons (or holes) are transported through the material and a proper understanding of this process is, thus, crucial to develop tailored properties.

Published under license by AIP Publishing

A fundamental precursor for understanding the macroscopic charge-transport behavior is to study ionization potentials (IPs) and electron affinities (EAs).[10] One approach to gain insight into these quantities is calculating frontier-orbital energies with density-functional theory (DFT). The advantage of conventional DFT is that it can be applied to ground-state properties of large systems due to its low scaling with system size. However, DFT lacks a systematic way to improve the functional and it is often not sufficiently accurate for properties such as bandgaps, excited-state energies, or charge-transport processes.[11–13] One way to improve over DFT is given by the many-body Green's function GW formalism.[14–21] The G_0W_0 method only involves a one-step evaluation instead of an iterative process, thus greatly reducing the computational costs while still improving significantly over DFT.[22–26] However, although in more accurate GW methods, the results are rather insensitive to the choice of the functional, and it is not the case for G_0W_0 in which the results are influenced by the initial choice of the functional.[27,28] Despite several advantages of the G_0W_0 method, e.g., the straightforward manner to obtain absolute IP/EA energies, it is more difficult to extract property information for the sought quasi-particle states.

An alternative to the GW approach is wavefunction methods as they can be systematically improved to the full configuration interaction (FCI) limit, and in general, they offer a straightforward way to investigate the target-state properties. Two approaches that have been successful in the last decades are the algebraic diagrammatic construction (ADC) scheme[29] and coupled-cluster (CC) response theory.[30–32] These methods, particularly the second-order approximate schemes, which have costs that scale with N^5, where N is a measure of the system size, have evolved into very efficient tools for studying the excited-state properties of medium-sized systems.[33–37] Another approach is given by the CIS(D_∞) method, which integrates the second-order perturbation theory into the configuration interaction singles (CIS) framework to improve its performance on calculating the excited state properties.[38] The accuracy and efficiency of CIS(D_∞), ADC(2), and second-order approximate coupled-cluster (CC2) singles and doubles are similar because of close technical relations.[39–41] Using wavefunction methods, a simple scheme to investigate electron-detachment and electron-attachment energies is used to calculate the energy difference between the ionic and the neutral system, which is also denoted the ΔE approach; see, e.g., Refs. 42 and 43. This scheme suffers from spin contamination when calculating the ions, and often, only the lowest ionic state can be investigated. In order to avoid spin contamination and to investigate higher ionic states, wavefunction methods can be combined with response theory or, in case of a coupled cluster, also with the equation-of-motion (EOM) ansatz to describe electron-detached or electron-attached states in which electrons are excited to the continuum or localized from the continuum to unoccupied MOs, respectively.[44–48]

Wavefunction methods have shown their ability to yield highly accurate results, but due to a rather steep scaling of the computational costs with system size, even dimers and trimers of medium-sized molecules are out of reach, in particular if excited-state properties are sought. In case of weakly interacting molecules, embedding approaches offer the advantage of *a priori* partitioning, leading to conceptual decomposition and significantly reduced computational scaling. There are numerous embedding methods each with a different approach on how to treat the subsystems. To give an example, one difference between embedding schemes is whether quantum mechanics (QM) methods are applied for the target subsystem only while classical molecular mechancis (MM) are employed for the environment, also denoted QM/MM, or the embedding scheme allows us to treat all subsystems at QM levels, also denoted QM/QM. Among all the QM/QM embedding schemes, frozen density embedding (FDE) is one efficient approach to study environment effects beyond pure Coulomb contributions on target molecules without the need of parameterization. For example, FDE allows both an accurate subsystem mode, in which all subsystems are treated with the same accuracy, and an embedding mode, in which more approximate methods are applied for the environment subsystems.[49–52] Recently, an equation-of-motion coupled-cluster singles and doubles for ionization potential (EOM-IP-CCSD) method combined with FDE for vertical transitions has been reported[53] in which DFT-in-DFT is used to obtain the embedding potential. EOM methods have also been developed recently in the framework of projector-based embedding.[54–56]

In the present work, we report the calculation of vertical as well as relaxed IP and EA energies in the presence of explicit molecular environments using FDE. This approach allows for an efficient calculation of ionized systems with a large size such as TAPP compounds, and the results obtained this way are more suitable for analyzing molecular properties.

This article is organized as follows. In Sec. II, the working equations, including the analytical nuclear gradients for ADC(2) and CIS(D_∞), are derived for the IP and EA approaches. In Sec. III, results obtained with the new implementation and the conceptual difference of supermolecular and embedding calculations are discussed. This article concludes with a short summary.

II. THEORY

A. Response equations for excitation energies

In coupled-cluster response theory, excitation energies are obtained as eigenvalues of the stability (Jacobian) matrix, which can be written for the standard CC models as, see e.g., Ref. 32,

$$A_{\mu\nu} = \langle \mu | \exp(-T)[H, \tau_\nu] \exp(T) | \mathrm{HF} \rangle, \tag{1}$$

where μ, ν denote the excitations out of the reference determinant $|\mathrm{HF}\rangle$. Using the convention that $a, b, c, \ldots$ are the virtual (unoccupied) and $i, j, k, \ldots$ are the occupied orbitals, the set of excitations becomes $\{\mu\} = \{ai, aibj, aibjck, \ldots\}$.

Due to the large dimension of **A**, excitation energies are obtained through a Davidson scheme in which the lowest excitation energies are obtained from linear combinations of trial vectors **R**. To determine the coefficients of the linear combinations, products with trial vectors are required to compute the residual for each trial vector,

$$\rho_\mu = \sum_\nu A_{\mu,\nu} R_\nu. \tag{2}$$

For the second-order approximate coupled cluster (CC2) singles and doubles method, the multiplication of the Jacobian **A** with a vector from the right is given for the closed-shell case as follows:[57]

Published under license by AIP Publishing

$$^{\mathrm{CC2}}\rho_a^i = \sum_b E_{ab}R_b^i - \sum_j R_a^j E_{ji} + \sum_{dl} \tilde{t}_{ad}^{il}\bar{F}_{ld} + \bar{F}'_{ai} + \sum_{dlc} \tilde{R}_{cd}^{il}(ld\hat{|}ac) - \sum_{dlk} \tilde{R}_{ad}^{kl}(ld\hat{|}ki) + \sum_{dl} \tilde{R}_{ad}^{il}\hat{F}_{ld}, \quad (3)$$

$$^{\mathrm{CC2}}\rho_{ab}^{ij} = (\varepsilon_a + \varepsilon_b - \varepsilon_i - \varepsilon_j)R_{ab}^{ij} + (ai\bar{|}bj), \quad (4)$$

with the following intermediates:

$$E_{ab} = \hat{F}_{ab} - \sum_{dlk} \tilde{t}_{ad}^{kl}(ld\hat{|}kb), \quad (5)$$

$$E_{ij} = \hat{F}_{ij} - \sum_{dlc} \tilde{t}_{cd}^{il}(ld\hat{|}jc), \quad (6)$$

$$\bar{F}_{kc} = \sum_{dl}[2(kc|ld) - (kd|lc)]R_d^l, \quad (7)$$

$$\bar{F}'_{ai} = \sum_{ck}[2(kc|ai) - (ki|ac)]R_c^k, \quad (8)$$

$$(ai\bar{|}bj) = \sum_c (ac\hat{|}bj)R_c^i + \sum_c (ai\hat{|}bc)R_c^j - \sum_k R_a^k(ki\hat{|}bj) - \sum_k R_b^k(ai\hat{|}kj). \quad (9)$$

In the present work, $\hat{F}_{pq}$ and $(pq\hat{|}rs)$ refer to the Fock-matrix elements and two-electron integrals of the similarity transformed Hamiltonian, $\exp(-T_1)H\exp(T_1)$, where T_1 is the single excitation part of the cluster operator. $\tilde{t}_{ab}^{ij}$ and $\tilde{R}_{ab}^{ij}$ denote the two times Coulomb minus the exchange combination of the ground-state and excited-state amplitudes, respectively.

In the present work, the resolution-of-identity (RI) approximation is applied; see, e.g., Refs. 58–60 and the references therein. The two-electron integrals are, therefore, computed from the following two-index and three-index integrals:

$$V_{PQ} = (P|Q), \quad (10)$$

$$B_{pq}^Q = \sum_{\alpha\beta P} C_{\alpha p}C_{\beta q}(\alpha\beta|P)V_{PQ}^{-1/2}, \quad (11)$$

$$\hat{B}_{pq}^Q = \sum_{\alpha\beta P} \Lambda_{\alpha p}^p \Lambda_{\beta q}^h(\alpha\beta|P)V_{PQ}^{-1/2}, \quad (12)$$

where $\mathbf{C}$ are the coefficients of the molecular orbitals (MOs), $\mathbf{V}^{-1/2}$ is the matrix inverse square root, and $(P|Q)$ and $(\alpha\beta|P)$ denote the Coulomb integrals. $\mathbf{\Lambda}^p$ and $\mathbf{\Lambda}^h$ are the usual T_1-transformed MOs, i.e., $\mathbf{\Lambda}^p = \mathbf{C}(\mathbf{1} - \mathbf{t}_1^T)$ and $\mathbf{\Lambda}^h = \mathbf{C}(\mathbf{1} + \mathbf{t}_1)$.

B. Continuum orbitals

As shown about two decades ago, ionization potentials can be obtained numerically for conventional linear-response methods when using a continuum orbital.[61] While in the original work an exponent of 10^{-50} was used, a diffuse coefficient of 10^{-10} yielded satisfying accuracy for the present purpose.

However, the continuum orbitals can not only be used to obtain IP and EA values numerically but they can also be used in a formal manner in the derivation of the methods, which then have eliminated the continuum orbital from the actual calculation. Continuum orbitals, denoted x in the following, have an orbital eigenvalue of exactly zero, i.e., $\hat{F}_{xx} = F_{xx} = \varepsilon_x = 0$, and they do not interact with the other orbitals located on the system so that all matrix elements of one-electron and two-electron integrals vanish, e.g., $F_{xq} = 0$, $\langle x|q\rangle = 0$, and $(xq|rs) = 0$. These properties are used in the following for the derivation, but the continuum orbitals are finally omitted in the resulting implementation.

C. Ionization potentials

1. Vertical ionization potentials

We relate the vertical ionization energies to vertical excitation energies where one electron is excited into an ultra-diffuse virtual orbital, denoted x in the following, with an energy of exactly zero and a vanishing overlap with the remaining basis functions centered on the investigated system. The excitation where one electron is excited into the vacuum orbital x is denoted as $\{\mu^h\} = \{xi, xibj, xibjck, \ldots\}$. Alternatively, the index is sometimes dropped, leading to the excitation hole manifold $\{\mu^h\} = \{i, ibj, ibjck, \ldots\}$, but in the present work, the index x is kept for a better readability. Since the electron in the orbital x cannot interact with the remaining system, $\mathbf{A}$ is the block diagonal with respect to the two excitation manifolds $\{\mu^h\}$ and $\{\mu\}\backslash\{\mu^h\}$. The ionization energies are, thus, obtained as the eigenvalues of the sub-block A_{μ^h,ν^h}.

To determine the eigenvalues of A_{μ^h,ν^h}, products with trial vectors of the following type are required:

$$\rho_{\mu^h} = \sum_{\nu^h} A_{\mu^h,\nu^h}R_{\nu^h}. \quad (13)$$

Replacing $\rho_a^i \to \rho_x^i$, $R_a^i \to R_x^i$, and $R_{ab}^{ij} \to R_{xb}^{ij}$ or $R_{ab}^{ij} \to R_{ax}^{ij}$ and restricting the ground-state amplitudes to excitations into the usual virtual basis functions, one obtains the following for the CC2 model:

$$^{\text{IP-CC2}}\rho_x^i = -\sum_j E_{ji}R_x^j - \sum_{dlk}(ld\hat{|}ki)\tilde{R}_{xd}^{kl} + \sum_{dl}\tilde{R}_{xd}^{il}\hat{F}_{ld}, \quad (14)$$

$$^{\text{IP-CC2}}\rho_{xb}^{ij} = (\varepsilon_b - \varepsilon_i - \varepsilon_j)R_{xb}^{ij} - \sum_k (ki\hat{|}aj)R_x^k. \quad (15)$$

The expressions for CIS(D_∞) are obtained from those for CC2 by replacing the ground-state amplitudes with the first-order Møller–Plesset (MP1) perturbation theory amplitudes as follows:

$$^{\text{IP-CIS}(D_\infty)}\rho_x^i = -\sum_j E_{ji}^{\mathrm{MP1}}R_x^j - \sum_{dlk}(ld|ki)\tilde{R}_{xd}^{kl}, \quad (16)$$

$$^{\text{IP-CIS}(D_\infty)}\rho_{xb}^{ij} = (\varepsilon_b - \varepsilon_i - \varepsilon_j)R_{xb}^{ij} - \sum_k (ki|aj)R_x^k. \quad (17)$$

The expressions for ADC(2) are obtained by symmetrizing in addition the contribution of what before has been the singles–singles block of the Jacobian matrix A_{μ^h,ν^h}. The effect of this is now reduced to a symmetrization of the contributions from $\mathbf{E}^{\mathrm{MP1}}$,

Published under license by AIP Publishing

$$ {}^{\text{IP-ADC(2)}}\rho_x^i = -\frac{1}{2}\sum_j (E_{ji}^{\text{MP1}} + E_{ij}^{\text{MP1}}) R_x^j - \sum_{dlk} (ld|ki)\tilde{R}_{xd}^{kl}, \quad (18) $$

$$ {}^{\text{IP-ADC(2)}}\rho_{xb}^{ij} = (\varepsilon_b - \varepsilon_i - \varepsilon_j) R_{xb}^{ij} - \sum_k (ki|aj) R_x^k. \quad (19) $$

2. Excited-state Lagrangian for CIS(D$_\infty$) and ADC(2)

Having obtained the eigenvalues and eigenvectors of the Jacobian, a Lagrange functional is constructed to facilitate the calculation of properties and analytical nuclear gradients of the ionized states,[62]

$$ \mathcal{L}^f = \langle \text{HF}|H + [H, T_2]|\text{HF}\rangle + \omega^f \left(1 - \sum_{\mu^h} \tilde{L}_{\mu^h}^f R_{\mu^h}^f\right) + \sum_{\mu^h \nu^h} \tilde{L}_{\mu^h}^f A_{\mu^h \nu^h} R_{\nu^h}^f + \sum_\mu \tilde{t}_\mu \Omega_\mu + \sum_{\mu_0} \tilde{\kappa}_{\mu_0} F_{\mu_0}, \quad (20) $$

where ω^f is the ionization energy and $\boldsymbol{\Omega}$ are the constraints for the amplitudes. The quantities $\tilde{\mathbf{t}}$, $\tilde{\mathbf{L}}$, and $\tilde{\boldsymbol{\kappa}}$ denote the amplitude multipliers, the excitation vector multipliers, and the orbital-rotation multipliers, respectively. Note that the Lagrange multipliers for the excited state, $\tilde{\mathbf{L}}^f$, refer to the hole manifold $\{\mu^h\}$, while the Lagrange multipliers for the ground-state amplitudes, $\tilde{\mathbf{t}}$, refer to the conventional manifold $\{\mu\}$. The index range of the Lagrange multipliers $\tilde{\kappa}_{\mu_0}$ depends on whether, e.g., a canonical, non-canonical, or semi-canonical representation is chosen; cf. Ref. 60.

In the present work, the ground-state embedding potential is used for both vertical transitions and nuclear gradients, that is, geometry relaxation. Note that the use of the ground-state embedding potential for geometry relaxation is an approximation as the environment densities are lacking polarization of the electron change, which results in a too little back-polarization of the ionized compound. The study of back-polarization effects is, however, beyond the scope of the present work and shall be addressed in future work.

3. Excited-state Lagrange multipliers

In order to make the Lagrangian stationary, the excited-state Lagrange multipliers $\tilde{\mathbf{L}}^f$ have to be determined. They are constructed to enforce a vanishing derivative with respect to the excitation vectors,

$$ \frac{\partial}{\partial R_{\mu^h}} \mathcal{L}^f = \sum_{\nu^h} \tilde{L}_{\nu^h}^f (A_{\nu^h \mu^h} - \omega^f) \stackrel{!}{=} 0, \quad (21) $$

which is expressed as an eigenvalue equation,

$$ \tilde{\mathbf{L}}^f \mathbf{A} = \omega^f \tilde{\mathbf{L}}^f. \quad (22) $$

The Lagrange multipliers are, thus, nothing else than the left eigenvectors. However, the biorthogonality condition is taken care of by explicitly enforcing $|\mathbf{R}^f| = 1$ and $\langle \mathbf{L}^f | \mathbf{R}^f \rangle = 1$ for $\mathbf{R}^f$ and $\mathbf{L}^f$, respectively.

For a transformation of the Jacobian A_{μ^h,ν^h} from the left, one obtains in a doubles-direct formulation only a residual ρ for the singles while the doubles are constructed on-the-fly,

$$ \rho_x^i = -\sum_j E_{ji} \tilde{L}_x^j - \sum_{dlk} (ld|ik) \tilde{L}_{dx}^{kl}, \quad (23) $$

$$ \tilde{L}_{ax}^{ij} = -\frac{2\sum_k \tilde{L}_x^k (j^p k^h | i^p a^h) - \sum_k \tilde{L}_x^k (i^p k^h | j^p a^h)}{\varepsilon_a - \varepsilon_i - \varepsilon_j}. \quad (24) $$

4. Ground-state amplitude multipliers

The equation that determines the ground-state amplitude multipliers is obtained by the differentiation of the Lagrangian with respect to the ground-state amplitudes t_λ,

$$ 0 \stackrel{!}{=} \frac{\partial}{\partial t_\lambda} \mathcal{L}^f = \left(\frac{\partial}{\partial t_\lambda} \langle \text{HF}|[H, T_2]|\text{HF}\rangle\right) + \sum_\mu \tilde{t}_\mu^f \left(\frac{\partial}{\partial t_\lambda} \Omega_\mu\right) + \sum_{\mu^h \nu^h} L_{\mu^h}^f \left(\frac{\partial}{\partial t_\lambda} A_{\mu^h \nu^h}\right) R_{\nu^h}^f. \quad (25) $$

In the latter equation, the first and second term on the right-hand side (RHS) are simply the conventional CC2 equations. Often, for the third term on the RHS, the following matrix $\mathbf{B}$ is introduced:

$$ B_{\mu^h,\nu^h;\lambda} = \frac{\partial}{\partial t_\lambda} A_{\mu^h \nu^h}. \quad (26) $$

However, for the models CIS(D$_\infty$) and ADC(2) in the present work, only the following contribution is needed:

$$ \sum_{ij} \tilde{L}_x^i B_{i,j;manb} R_x^j = -\frac{\partial}{\partial t_{ab}^{mn}} \sum_{ij} \tilde{L}_x^i E_{ji} R_x^j = -2\sum_j \tilde{L}_x^m (nb|ja) R_x^j + \sum_j \tilde{L}_x^m (na|jb) R_x^j. \quad (27) $$

5. Z-vector equation and gradient

In order to compute the orbital-relaxed excited-state properties, the Lagrangian also has to be stationary with respect to the ground-state orbital rotations. The respective equations are obtained by differentiating

$$ 0 \stackrel{!}{=} \frac{\partial}{\partial \kappa_{\mu_0}} \mathcal{L}^f = \left(\frac{\partial}{\partial \kappa_{\mu_0}} \langle \text{HF}|H + [H, T_2]|\text{HF}\rangle\right) + \sum_{\mu\nu^h} L_{\mu^h}^f \left(\frac{\partial}{\partial \kappa_{\mu_0}} A_{\mu^h \nu^h}\right) R_{\nu^h}^f + \sum_\mu \tilde{t}_\mu \left(\frac{\partial}{\partial \kappa_{\mu_0}} \Omega_\mu\right) + \sum_{\mu_0} \tilde{\kappa}_{\mu_0} \left(\frac{\partial}{\partial \kappa_{\mu_0}} F_{\mu_0}\right). \quad (28) $$

TABLE I. Transformation matrices in case of IP and EA matrices required to compute the intermediates. Note that all other Λ_i and Λ_a are zero in case of excited-state contributions for both IPs and EAs.

	IP	EA
$\tilde{\Lambda}_x^p =$	$-\sum_j C_j R_x^j$	0
$\tilde{\Lambda}_x^h =$	0	$\sum_b C_b R_b^x$
$\check{\Lambda}_x^p =$	0	$\sum_b \Lambda_b^p L_b^x$
$\check{\Lambda}_x^h =$	$-\sum_j \Lambda_j^h L_x^j$	0

Published under license by AIP Publishing

TABLE II. Intermediates for analytical nuclear gradients in the IP case.

Three-center integrals	Level 1 intermediates
$\tilde{B}^Q_{xq} = \sum_{\alpha\beta P} \tilde{\Lambda}^p_{\alpha x} \Lambda^h_{\beta q} (\alpha\beta\|P) V^{-1/2}_{PQ}$	$Y^Q_{xi}(R) = \sum_{jb} \tilde{R}^{ij}_{xb} B^Q_{jb}$
$\check{B}^Q_{px} = \sum_{\alpha\beta P} \Lambda^p_{\alpha p} \check{\Lambda}^h_{\beta x} (\alpha\beta\|P) V^{-1/2}_{PQ}$	$\tilde{Y}^Q_{ai}(R) = \sum_{j} \tilde{R}^{ij}_{ax} \check{B}^Q_{jx}$
$\check{\tilde{B}}^Q_{ia} = -\sum_k L^i_x R^k_x B^Q_{ka}$	$\check{\tilde{Y}}^Q_{ai}(t) = \sum_{jb} \tilde{t}^{ij}_{ab} \check{\tilde{B}}^Q_{jb}$
	$\check{Y}^Q_{ai}(L) = \sum_{j} L^{ij}_{ax} \tilde{B}^Q_{xj}$
Level 2 intermediates	**Level 3 intermediates**
${}^A\tilde{Y}^P_{pj} = Y^P_{xj}(R)\check{\lambda}^h_{px} + \sum_a {}^A\Delta^P_{ja} \lambda^h_{pa}$	${}^A\Gamma^{(a),Q}_{j\beta} = \sum_p C_{\beta p} \sum_P V^{-1/2A}_{PQ} \tilde{Y}^P_{pj}$
${}^A\Delta^P_{jb} = \tilde{Y}'^P_{bj}(t) + \tilde{Y}^P_{bj}(R)$	${}^A\Gamma^{(b),Q}_{x\beta} = 0$
$\tilde{Y}'^P_{ai}(t) = \tilde{Y}^P_{ai}(t) - \sum_k (L^i_x R^k_x) Y^Q_{ak}(t)$	${}^A\tilde{\Gamma}^{(b),Q}_{j\beta} = \sum_P V^{-1/2}_{PQ} \left(\sum_a \Lambda^p_{\beta a} \check{Y}^P_{aj}(L) + \sum_a \tilde{\Lambda}^p_{\beta x} \check{Y}^P_{xj}(L) \right)$
${}^A\overset{\star}{Y}{}^P_{px} = 0$	${}^A\Gamma^{(c),Q}_{x\beta} = 0$

Re-arranging yields the following well-known Z-vector equation:

$$-\sum_{\mu_0} \tilde{\kappa}_{\mu_0} \left(\frac{\partial}{\partial \kappa_{\mu_0}} F_{\mu_0} \right) = \left(\frac{\partial}{\partial \kappa_{\mu_0}} \langle \mathrm{HF}|H + [H, T_2]|\mathrm{HF}\rangle \right) + \sum_{\mu^h \nu^h} L^f_{\mu^h} \left(\frac{\partial}{\partial \kappa_{\mu_0}} A_{\mu^h \nu^h} \right) R^f_{\nu^h} + \sum_{\mu} \tilde{t}^f_{\mu} \left(\frac{\partial}{\partial \kappa_{\mu_0}} \Omega_{\mu} \right). \tag{29}$$

Using the effective densities, the occupied-virtual block on the right-hand side can be expressed as:

$$\eta_{AI} = \frac{1}{2} \left(D^{\mathrm{F,ex}}_{AI} + D^{\mathrm{F,ex}}_{IA} \right) (\varepsilon_I - \varepsilon_A) - \frac{1}{4} \left(D^{\mathrm{F,ex}}_{pq} + D^{\mathrm{F,ex}}_{qp} \right) A_{pqAI} + ({}^{\mathrm{ex}}H_{AI} - {}^{\mathrm{ex}}\Omega_{AI} - {}^{\mathrm{ex}}H_{IA} + {}^{\mathrm{ex}}\Omega_{IA}), \tag{30}$$

where the indices I, J and A, B denote the general, i.e., active and frozen, occupied and virtual indices, respectively. The only difference to Refs. 36 and 63 is that densities employing the particle/hole excitation vectors are used. For example, the one-electron density $\mathbf{D}^{F,A}$ is defined in the IP case as follows (for zero T_1 amplitudes):

$$D^{F,A}_{ij} = -L^i_x R^j_x - \sum_{ak} L^{jk}_{ax} R^{ik}_{ax}, \tag{31}$$

$$D^{F,A}_{ia} = \tilde{C}_{ai} = \sum_j \tilde{R}^{ij}_{ax} L^j_x, \tag{32}$$

$$D^{F,A}_{ai} = 0, \tag{33}$$

$$D^{F,A}_{aa} = \sum_{ij} L^{ij}_{ax} R^{ij}_{ax}, \tag{34}$$

while the ground-state densities such as $\mathbf{D}^{\xi}$ remain unchanged. Similarly, the matrices ${}^{\mathrm{ex}}\mathbf{H}$ and ${}^{\mathrm{ex}}\mathbf{\Omega}$ are given as

$${}^{\mathrm{ex}}\mathbf{H} = \sum_{abc} {}^{\xi}\mathbf{H}^{(x)} + \sum_{ab} {}^{A}\mathbf{H}^{(x)}, \tag{35}$$

$${}^{\mathrm{ex}}\mathbf{\Omega} = \sum_{abc} {}^{\xi}\mathbf{\Omega}^{(x)} + \sum_{abc} {}^{A}\mathbf{\Omega}^{(x)}, \tag{36}$$

for which the ground-state contributions, ${}^{\xi}\mathbf{H}^{(x)}$ and ${}^{\xi}\mathbf{\Omega}^{(x)}$, remain unaltered compared to the conventional excited-state case.

Finally, the contributions are computed from the matrices ${}^{A}\mathbf{H}$ and ${}^{A}\mathbf{\Omega}$, which are given in the case of IP-ADC(2), as follows, c.f., Tables I and II:

$${}^A H^{(a)}_{pq} = \sum_{Qi} {}^A\tilde{Y}^Q_{pi} B^Q_{iq}, \tag{37}$$

$${}^A H^{(b)}_{pq} = \sum_a \delta_{pa} \sum_{Qi} \check{Y}^Q_{ai} \sum_r \delta^h_{ri} B^Q_{qr} + \tilde{\lambda}^p_{px} \sum_{Qi} \check{Y}^Q_{xi} \sum_r \delta^h_{ri} B^Q_{qr}, \tag{38}$$

$${}^A\Omega^{(a)}_{pq} = \sum_{\alpha} C_{\alpha q} \sum_j \delta_{pj} \sum_{Q\beta} {}^A\Gamma^{(a),Q}_{j\beta} (\alpha\beta|Q), \tag{39}$$

$${}^A\Omega^{(b)}_{pq} = \sum_{\alpha} C_{\alpha q} \sum_j \delta^h_{pj} \sum_{Q\beta} {}^A\tilde{\Gamma}^{(b),Q}_{j\beta} (\alpha\beta|Q). \tag{40}$$

D. Electron attachment

1. Vertical electron attachment energies

Similar to the IP case, vertical electron attachment energies are related to vertical excitation energies where one electron is excited from an ultra-diffuse occupied orbital, x (*vide supra*), with

Published under license by AIP Publishing

TABLE III. Intermediates for analytical nuclear gradients in the EA case.

Three-center integrals	Level 1 intermediates
$\tilde{B}^Q_{px} = \sum_{\alpha\beta P} \Lambda^p_{\alpha p} \tilde{\Lambda}^h_{\beta x} (\alpha\beta\|P) V^{-1/2}_{PQ}$	$Y^Q_{ax}(R) = \sum_{jb} \tilde{R}^{xj}_{ab} B^Q_{jb}$
$\check{B}^Q_{xq} = \sum_{\alpha\beta P} \check{\Lambda}^p_{\alpha x} \Lambda^h_{\beta q} (\alpha\beta\|P) V^{-1/2}_{PQ}$	$\tilde{Y}^Q_{ai}(R) = \sum_{b} \tilde{R}^{ix}_{ab} \check{B}^Q_{xb}$
$\check{\tilde{B}}^Q_{ia} = -\sum_{c} L^x_a R^x_c B^Q_{ic}$	$\tilde{\tilde{Y}}^Q_{ai}(t) = \sum_{jb} \tilde{t}^{ij}_{ab} \check{\tilde{B}}^Q_{jb}$
	$\check{Y}^Q_{ai}(L) = \sum_{b} L^{ix}_{ab} \tilde{B}^Q_{bx}$
Level 2 intermediates	**Level 3 intermediates**
${}^A\tilde{\tilde{Y}}^P_{pj} = \sum_a {}^A\Delta^P_{ja} \lambda^h_{pa}$	${}^A\Gamma^{(a),Q}_{j\beta} = \sum_p C_{\beta p} \sum_P V^{-1/2A}_{PQ} \tilde{\tilde{Y}}^P_{pj}$
${}^A\Delta^P_{jb} = \tilde{\tilde{Y}}'^P_{bj}(t) + \tilde{Y}^P_{bj}(R)$	${}^A\Gamma^{(b),Q}_{x\beta} = \sum_a \Lambda^p_{\beta a} \sum_P V^{-1/2}_{PQ} \check{Y}^P_{ax}(L)$
$\tilde{\tilde{Y}}'^P_{ai}(t) = \tilde{\tilde{Y}}^P_{ai}(t) - \sum_c (L^x_c R^x_a) Y^Q_{ci}(t)$	${}^A\bar{\Gamma}^{(b),Q}_{j\beta} = \sum_P V^{-1/2}_{PQ} \sum_a \Lambda^p_{\beta a} \check{\tilde{Y}}^P_{aj}(L)$
${}^A\overset{\star}{Y}{}^P_{px} = \sum_b Y^P_{bx}(R) \lambda^h_{pb}$	${}^A\Gamma^{(c),Q}_{x\beta} = \sum_p C_{\beta p} \sum_P V^{-1/2A}_{PQ} \overset{\star}{Y}{}^P_{px}$

an energy of exactly zero and a vanishing overlap with the remaining basis functions centered on the investigated system, into a virtual orbital of the system. The excitation where one electron is excited from x is denoted as $\{\mu^p\} = \{ax, axbj, axbjck, \ldots\}$. Similar to the IP case, the index can be dropped, resulting in $\{\mu^p\} = \{a, abj, abjck, \ldots\}$, but for a better readability, the index x is kept in the present work. Since the electron in the orbital x cannot interact with the remaining system, $\mathbf{A}$ is again a block diagonal with respect to the two excitation manifolds $\{\mu^p\}$ and $\{\mu\} \setminus \{\mu^p\}$. The electron attachment energies are, thus, obtained as the eigenvalues of the sub-block A_{μ^p,ν^p}.

To determine the eigenvalues of A_{μ^p,ν^p}, products with trial vectors of the following type are required:

$$\rho_{\mu^p} = \sum_{\nu^p} A_{\mu^p,\nu^p} R_{\nu^p}. \tag{41}$$

Replacing one of the occupied indices of the trial vector and one of the occupied indices of the result vector by x in the expressions for excitation energies, and restricting the ground-state amplitudes to excitation from the usual occupied orbitals with $i \neq x$, one obtains

$${}^{\text{EA-CC2}}\rho^x_a = \sum_b E_{ab} R^x_b + \sum_{dlc} \tilde{R}^{xl}_{cd} (ld|\hat{ac}) + \sum_{dl} \tilde{R}^{xl}_{ad} \hat{F}_{ld}, \tag{42}$$

$${}^{\text{EA-CC2}}\rho^{xj}_{ab} = (\varepsilon_a + \varepsilon_b - \varepsilon_j) R^{xj}_{ab} + \sum_c (ac|\hat{bj}) R^x_c. \tag{43}$$

The expressions for CIS(D_∞) are obtained from the CC2 equations by replacing the ground-state amplitudes with the first-order Møller–Plesset (MP1) perturbation theory amplitudes as follows:

$${}^{\text{EA-CIS}(D_\infty)}\rho^x_a = \sum_b E^{\text{MP1}}_{ab} R^x_b + \sum_{dlc} \tilde{R}^{xl}_{cd} (ld|ac), \tag{44}$$

$${}^{\text{EA-CIS}(D_\infty)}\rho^{xj}_{ab} = (\varepsilon_a + \varepsilon_b - \varepsilon_j) R^{xj}_{ab} + \sum_c (ac|bj) R^x_c. \tag{45}$$

The expressions for ADC(2) are obtained by symmetrizing in addition the contribution of what before has been the singles–singles block of the Jacobian matrix A_{μ^p,ν^p}. The effect of this is now reduced to a symmetrization of the contributions from $\mathbf{E}^{\text{MP1}}$,

$${}^{\text{EA-ADC(2)}}\rho^x_a = \frac{1}{2} \sum_b (E^{\text{MP1}}_{ab} + E^{\text{MP1}}_{ba}) R^x_b + \sum_{dlc} \tilde{R}^{xl}_{cd} (ld|ac), \tag{46}$$

$${}^{\text{EA-ADC(2)}}\rho^{xj}_{ab} = (\varepsilon_a + \varepsilon_b - \varepsilon_j) R^{xj}_{ab} + \sum_c (ac|bj) R^x_c. \tag{47}$$

2. Excited-state Lagrangian for CIS(D_∞) and ADC(2)

Having obtained the eigenvalues and eigenvectors of the Jacobian, a Lagrange functional is constructed to facilitate the calculation of the properties and analytical nuclear gradients of the electron-attached states,[62]

$$\mathcal{L}^f = \langle \text{HF}|H + [H, T_2]|\text{HF}\rangle + \omega^f \left(1 - \sum_{\mu^p} \bar{L}^f_{\mu^p} R^f_{\mu^p}\right) + \sum_{\mu^p \nu^p} \bar{L}^f_{\mu^p} A_{\mu^p \nu^p} R^f_{\nu^p} + \sum_{\mu} \bar{t}_\mu \Omega_\mu + \sum_{\mu_0} \bar{\kappa}_{\mu_0} F_{\mu_0}, \tag{48}$$

where ω^f is the electron-attachment energy. Note that the Lagrange multipliers for the excited state, $\bar{\mathbf{L}}^f$, refer to the particle manifold $\{\mu^p\}$ in the EA case.

In order to make the Lagrangian stationary, the excited-state Lagrange multipliers $\bar{\mathbf{L}}^f$ have to be determined, which are, similar to the IP case, given as the left eigenvectors of the Jacobian A_{μ^p,ν^p}. We, therefore, follow the same approach as for IPs and just replace the μ^h manifold with the μ^p manifold, which leads to the following non-vanishing contributions to $\bar{L}^{xj}_{ab}$:

$$\bar{L}^{xj}_{ab} = \frac{2\sum_c (ca|jb) \bar{L}^x_c - \sum_c (cb|ja) \bar{L}^x_c}{\varepsilon_b + \varepsilon_a - \varepsilon_j}. \tag{49}$$

Similar to the IP case, the ground-state amplitudes are obtained by the differentiation of the Lagrangian with respect to the ground-state amplitudes t_λ. Following an analogous derivation as for IPs, for the models EA-CIS(D_∞) and EA-ADC(2), the doubles contribution is obtained as follows:

$$\sum_{cd} \bar{L}^x_c B_{c,d;manb} R^x_d = \frac{\partial}{\partial t^{mn}_{ab}} \sum_{cd} \bar{L}^x_c E_{cd} R^x_d = -2 \sum_d \bar{L}^x_a (nb|md) R^x_d + \sum_d \bar{L}^x_b (na|md) R^x_d. \tag{50}$$

3. Z-vector equation and gradient

In case of EA methods, differentiating and rearranging yield a corresponding Z-vector equation and right-hand side; cf. Eq. (30).

Published under license by AIP Publishing

The difference is located in the effective densities, which are now constructed from the particle vectors,

$$D^{F,A}_{ij} = -\sum_{ab} L^{xj}_{ab} R^{ix}_{ab}, \tag{51}$$

$$D^{F,A}_{ia} = \bar{C}_{ai} = \sum_{xb} \tilde{R}^{ix}_{ab} L^{x}_{b}, \tag{52}$$

$$D^{F,A}_{ai} = 0, \tag{53}$$

$$D^{F,A}_{ab} = L^{x}_{a} R^{x}_{b} + \sum_{ic} L^{ix}_{ac} R^{ix}_{bc}. \tag{54}$$

The ground-state contributions, e.g., $\mathbf{D}^{\xi}$, remain unchanged, while the matrices needed for the right-hand side vector $\boldsymbol{\eta}$ are given as, c.f., Tables I and III,

$${}^{A}H^{(a)}_{pq} = \sum_{Qi} {}^{A}\tilde{\bar{Y}}^{Q}_{pi} B^{Q}_{iq}, \tag{55}$$

$${}^{A}H^{(b)}_{pq} = \sum_{a} \lambda^{p}_{pa} \sum_{Qx} \check{Y}^{Q}_{ax} \sum_{r} \bar{\lambda}^{h}_{rx} B^{Q}_{qr} + \sum_{a} \lambda^{p}_{pa} \sum_{Qi} \check{\bar{Y}}^{Q}_{ai} \sum_{r} \lambda^{h}_{ri} B^{Q}_{qr}, \tag{56}$$

$${}^{A}H^{(c)}_{pq} = \sum_{Qx} \overset{\star}{Y}{}^{Q}_{px} \sum_{r} \check{\lambda}^{p}_{rx} B^{Q}_{rq} \tag{57}$$

and

$${}^{A}\Omega^{(a)}_{pq} = \sum_{\alpha} C_{\alpha q} \sum_{j} \lambda^{p}_{pj} \sum_{Q\beta} {}^{A}\Gamma^{(a),Q}_{j\beta}(\alpha\beta|Q), \tag{58}$$

$${}^{A}\Omega^{(b)}_{pq} = \sum_{\alpha} C_{\alpha q} \sum_{j} \lambda^{h}_{pj} \sum_{Q\beta} {}^{A}\bar{\Gamma}^{(b),Q}_{j\beta}(\alpha\beta|Q) + \sum_{\alpha} C_{\alpha q} \sum_{j} \bar{\lambda}^{h}_{px} \sum_{Q\beta} {}^{A}\Gamma^{(b),Q}_{x\beta}(\alpha\beta|Q), \tag{59}$$

$${}^{A}\Omega^{(c)}_{pq} = \sum_{\alpha} C_{\alpha q} \sum_{x} \check{\lambda}^{p}_{px} \sum_{Q\beta} {}^{A}\Gamma^{(c),Q}_{x\beta}(\alpha\beta|Q). \tag{60}$$

Some of these quantities are also used to compute the gradient itself. To give an example, the differentiated three-index integrals are contracted with an intermediate $\boldsymbol{\Delta}^{\mathrm{ao}}$,

$$\frac{dL}{d\chi} \leftarrow \sum_{\alpha\beta P} \Delta^{P,ao}_{\alpha\beta} \frac{\partial(\alpha\beta|P)}{\partial\chi}. \tag{61}$$

For this contribution, the intermediate $\boldsymbol{\Delta}^{\mathrm{ao}}$ has to be contracted as follows for the excited-state contributions:

$$\Delta^{P,ao}_{\alpha\beta} \leftarrow \sum_{j} \Big(C_{\alpha j} {}^{A}\Gamma^{(a),Q}_{j\beta} + {}^{A}\bar{\Gamma}^{(b),Q}_{j\alpha} \Lambda^{h}_{\beta j} \Big) + \Big({}^{A}\Gamma^{(b),Q}_{x\alpha} \bar{\Lambda}^{h}_{\beta x} + \check{\Lambda}^{p}_{\alpha x} {}^{A}\Gamma^{(c),Q}_{x\beta} \Big). \tag{62}$$

E. Frozen-density embedding

Employing the *a priori* partitioning of FDE, the total electron density is constructed as the sum of the subsystem electron densities,

$$\rho(\mathbf{r}) = \sum_{z} \rho_z(\mathbf{r}). \tag{63}$$

Each subsystem density ρ_z is obtained from individual subsystem calculations in which the polarization of the subsystems is obtained via an effective potential, *vide infra*. Due to such a partitioning, the energy can be expressed as follows for two subsystems, I and II:

$$E_{\mathrm{tot}}[\rho(\mathbf{r})] = E_{\mathrm{I}}[\rho_{\mathrm{I}}(\mathbf{r})] + E_{\mathrm{int}}[\rho_{\mathrm{I}}(\mathbf{r}), \rho_{\mathrm{II}}(\mathbf{r})] + E_{\mathrm{II}}[\rho_{\mathrm{II}}(\mathbf{r})], \tag{64}$$

where the interaction between the subsystems is given as[64]

$$E_{\mathrm{int}}[\rho_{\mathrm{I}}, \rho_{\mathrm{II}}] = \int \rho_{\mathrm{I}}(\mathbf{r}) v^{\mathrm{II}}_{\mathrm{nuc}}(\mathbf{r}) \mathrm{d}\mathbf{r} + \int \rho_{\mathrm{II}}(\mathbf{r}) v^{\mathrm{I}}_{\mathrm{nuc}}(\mathbf{r}) \mathrm{d}\mathbf{r} + E^{\mathrm{I,II}}_{\mathrm{nuc}} + \iint \frac{\rho_{\mathrm{I}}(\mathbf{r}) \rho_{\mathrm{II}}(\mathbf{r}')}{|\mathbf{r} - \mathbf{r}'|} \mathrm{d}\mathbf{r}\, \mathrm{d}\mathbf{r}' + E^{\mathrm{nadd}}_{\mathrm{emb:xck}}[\rho_{\mathrm{I}}, \rho_{\mathrm{II}}]. \tag{65}$$

In the FDE approach, the non-additive exchange-correlation and the kinetic energy contributions are expressed using density-functional theory (DFT), independently of the actual subsystem methods, and read as follows:

$$E^{\mathrm{nadd}}_{\mathrm{emb:xck}}[\rho_{\mathrm{I}}, \rho_{\mathrm{II}}] = E_{\mathrm{xc}}[\rho_{\mathrm{I}} + \rho_{\mathrm{II}}] - \sum_{z=\mathrm{I,II}} E_{\mathrm{xc}}[\rho_z] + T_s[\rho_{\mathrm{I}} + \rho_{\mathrm{II}}] - \sum_{z=\mathrm{I,II}} T_s[\rho_z]. \tag{66}$$

The polarization of the subsystems is introduced by including an effective embedding potential in the individual subsystem calculations, which is obtained, due to the DFT formalism, as the functional derivative of the interaction energy,

$$v^{\mathrm{emb,I}}(\mathbf{r}) = \left. \frac{\delta E_{\mathrm{int}}[\rho]}{\delta\rho(\mathbf{r})} \right|_{\rho=\rho_{\mathrm{I}}}. \tag{67}$$

In order to construct a supermolecular Lagrangian in the framework of FDE, the interaction energy E_{int} and the environment energy E_{II} are added to Eq. (20) or Eq. (48). As discussed earlier,[65,66] however, we neglect the environment contributions of E_{II} in the spirit of uncoupled FDE (FDEu). The FDEu-ADC(2) Lagrange functional can then be written as

$$\mathcal{L}^{f}_{\mathrm{ADC(2),exc,FDEu}} = \langle \mathrm{HF}|H|\mathrm{HF}\rangle + \sum_{pq} \Big(D^{\mathrm{F,ex},f}_{pq} + D^{\kappa}_{pq} \Big) \mathrm{F}_{pq} + \frac{1}{2} \sum_{pqrs} \Big(d^{\mathrm{nsep},\xi,f}_{pqrs} + d^{\mathrm{nsep,A},f}_{pqrs} \Big) \times (pq|rs)_{\mathrm{DF}} + E_{\mathrm{int}}, \tag{68}$$

where the Fock matrix $\mathbf{F}$ contains the embedding potential,

$$F_{pq} = F^{\mathrm{vac}}_{pq} + v^{\mathrm{emb}}_{pq}. \tag{69}$$

Once the molecular orbital (MO) coefficients, coupled cluster amplitudes, multipliers, and excitation vectors, as well as the Lagrange multipliers for the orbital rotations, are computed, the gradient can

Published under license by AIP Publishing

be obtained as the partial derivative of the total Lagrangian, Eq. (68), with respect to the displacement of the nuclear coordinates of the active subsystem $\vec{\mathbf{X}}$,

$$\begin{aligned}\frac{\mathrm{d}\mathcal{L}_{\mathrm{ADC(2),exc,FDEu}}}{\mathrm{d}\vec{\mathbf{X}}} &= \frac{\partial \mathcal{L}_{\mathrm{ADC(2),exc}}}{\partial \vec{\mathbf{X}}} - \sum_{pq} \mathrm{F}^{\mathrm{eff,\,emb}}_{pq} S^{[\vec{X}]}_{pq} \\ &+ \left(\frac{\partial}{\partial \vec{X}} E^{\mathrm{I,II}}_{\mathrm{nuc}}\right) + \int \rho_{\mathrm{II}}(\mathbf{r}) \left(\frac{\partial}{\partial \vec{X}} v^{\mathrm{I}}_{\mathrm{nuc}}(\mathbf{r})\right) \mathrm{d}\mathbf{r} \\ &+ \sum_{pq} D^{\mathrm{HF}}_{pq} \langle p | v^{\mathrm{I}}_{\mathrm{emb:coul}} | q \rangle^{[\vec{X}]} \\ &+ 2 \sum_{pq} D^{\mathrm{HF}}_{pq} \langle p^{[\vec{X}]} | v^{\mathrm{I}}_{\mathrm{emb:xck}} | q \rangle \\ &+ \sum_{pq} (D^{\mathrm{F,ex}}_{pq} + D^{\kappa}_{pq}) \langle p | v^{\mathrm{I}}_{\mathrm{emb}} | q \rangle^{[\vec{X}]}. \end{aligned} \tag{70}$$

Here, $\mathbf{F}^{\mathrm{eff}}$ is the effective Fock matrix, which accounts for the metric change upon geometric perturbations of the underlying Gaussian basis functions. The analytical nuclear excited-state gradients for conventional ADC(2), $\frac{\partial \mathcal{L}^{J}_{\mathrm{ADC(2),exc}}}{\partial \vec{\mathbf{X}}}$, are given for the formalism used in the present work in Refs. 36 and 40.

III. RESULTS

After providing the computational details in Sec. III A, in Secs. III B and III C, reference systems are investigated to assess the accuracy obtained with the analytical gradients and, in particular, the effect of the charge localization in the dimers using the FDE ansatz. In Sec. III D, the new methods are applied to TAPP compounds, which are used as organic semiconductors.

A. Computational details

Unless stated otherwise, all calculations, in particular all FDE calculations, are carried out using KOALA,[67,68] which employs density fitting, also abbreviated as RI,[58–60] using the self-consistent field (SCF) density in the embedding potential. The embedding exchange-correlation functional used was Perdew-Burke-Ernzerhof (PBE),[69] and the embedding kinetic energy functional used was PW91k.[70] Electron-detachment (IP) calculations were performed using the def2-TZVP basis set,[71] and electron attachment (EA) calculations for neutral systems were performed with the def2-TZVPD basis set to account for accurate virtual orbitals.[72] In case of geometry-relaxed transitions, only the subsystem which is excited is relaxed, while all other subsystems' geometries are kept frozen.

In the present work, electron attachment energies are provided as $\Delta E_{\mathrm{attachment}} = -E_{\mathrm{EA}}$ in order to distinguish them more easily in the tables from the ionization potentials. We have, therefore, adapted also the sign of the experimental adiabatic electron affinity (AEA) value of azulene to -0.8 ± 0.1 eV accordingly.[73,74]

1. Reference values

Reference results at the ΔCCSD(T) level of theory were obtained using TURBOMOLE.[75,76] In order to avoid problems due to spin contamination, in addition, results using a continuum orbital at the coupled-cluster singles and doubles (CCSD) level of theory are reported. For these numerical calculations, a continuum orbital with an exponent of 10^{-10} was used and has been checked using the CFOUR program[77] to confirm the use of the RI approximation. In case of IP calculations, the target state is the one which is dominated by the excitation from the HOMO to the continuum orbital. In case of EA calculations, two additional electrons were included in the calculation, leading to an occupation of the continuum orbital with two electrons. The EA value was then determined as the singlet excitation, which is dominated by the transition from the continuum orbital into the valence LUMO of the molecular system.

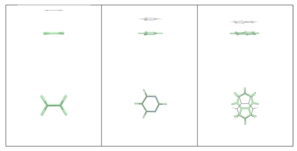


FIG. 1. Side view (top) and top view (bottom) of ethylene dimer (left), pyrimidine dimer (middle), and azulene dimer (right), at an intermolecular distance of 3Å.

B. Ionization potentials

In order to assess the accuracy of the present approach employing FDE, ethylene and pyrimide and selected dimers are computed, see Fig. 1, for which results are presented in Table IV, including the results from the reference methods. Ethylene and pyrimide were chosen to investigate the performance on two structures that can be considered the basic building blocks of, e.g., TAPPs.

Starting with the monomer ethylene molecule, Table IV shows that the methods IP-CIS(D_∞), IP-ADC(2), and IP-CC2 yield a sufficient agreement within 0.05 eV. The reference methods, i.e., CCSD and ΔCCSD(T), agree among each other within 0.02 eV, which points to a small influence of the triples. The reference values differ to the second-order approximate methods by about 0.55 eV, which is in agreement with a benchmark study.[79] However, in case of supermolecular calculations on the dimers, the second-order methods are able to reproduce the distance dependence of the reference methods. For example, in case of IP-ADC(2) at 3.0 Å distance, a shift of −1.36 eV with respect to the monomer is obtained, which shows a reduced deviation of about 0.04 eV to the shift obtained with CCSD, which is computed to be −1.32 eV.

In case of pyrimidine, the ΔCCSD(T) is not a sufficiently accurate reference method since the spin contamination at the SCF level of theory becomes significantly large; see Table IV. However, the vertical IP of the monomer, obtained from numerical CCSD, exhibits a deviation of about 1 eV to IP-ADC(2) and IP-CC2. Table IV

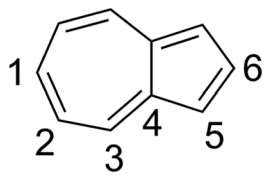


FIG. 2. Lewis representation of the azulene molecule.

Published under license by AIP Publishing

TABLE IV. Ethylene and pyrimidine dimer vertical ionization potentials in eV calculated with different methods as implemented in the KOALA program with and without embedding. Values in parentheses denote the shift with respect to the corresponding monomer in the corresponding method. The experimental ionization potential for pyrimidine is 9.8 eV.[78]

Molecule	System	Distance (Å)	IP-CIS(D_∞)	IP-ADC(2)	IP-CC2	CCSD	ΔCCSD(T)
Ethylene dimer	Superm.	3.0	8.91 (−1.36)	8.91 (−1.36)	8.87 (−1.35)	9.30 (−1.32)	9.30 (−1.29)
		5.0	10.09 (−0.18)	10.09 (−0.18)	10.05 (−0.17)	10.45 (−0.17)	10.44 (−0.15)
		7.5	10.24 (−0.03)	10.24 (−0.03)	10.19 (−0.03)	10.59 (−0.03)	10.57 (−0.02)
	FDE	3.0	10.01 (−0.26)	10.01 (−0.26)	9.96 (−0.26)		
		5.0	10.19 (−0.08)	10.19 (−0.08)	10.14 (−0.08)		
		7.5	10.24 (−0.03)	10.24 (−0.03)	10.20 (−0.02)		
	Monomer		10.27	10.27	10.22	10.62	10.59
Pyrimidine dimer	Superm.	3.0	8.23 (−0.45)	8.23 (−0.45)	8.17 (−0.43)		
		5.0	8.59 (−0.09)	8.59 (−0.09)	8.52 (−0.08)		
		7.5	8.65 (−0.03)	8.65 (−0.03)	8.58 (−0.02)		
	FDE	3.0	8.57 (−0.11)	8.57 (−0.11)	8.49 (−0.11)		
		5.0	8.63 (−0.05)	8.63 (−0.05)	8.56 (−0.04)		
		7.5	8.66 (−0.02)	8.66 (−0.02)	8.58 (−0.02)		
	Monomer		8.68	8.68	8.60	9.73	10.57[a]

[a] $\langle S^2 \rangle_{SCF} = 0.917$.

furthermore shows that the interaction in the pyrimidine dimer is significantly less pronounced compared to ethylene since the supermolecular IP at a distance of 3 Å is 8.22 eV, which differs from the monomer value of 8.71 eV by less than 0.5 eV.

Finally, Table IV also contains values for dimers obtained by employing the FDE ansatz. Comparing these values to the supermolecular dimer calculations, it can be seen that with increasing distance, the supermolecular calculations and the FDE approach both converge smoothly to the monomer result. For the rather short distance of 3 Å, the supermolecular calculations and the FDE results differ by almost 1 eV in case of ethylene. The reason for this is rooted in the FDE ansatz itself, which localizes the charge on one fragment, while in case of the supermolecular calculations, the charge is evenly distributed among the two molecules. An analysis in terms of atomic charges is carried out for the EA approach; see Sec. III C.

1. Geometry relaxation

Having assessed the accuracy of the methods for vertical transitions, we now turn to adiabatic transitions for relaxed geometries, that is, the relaxed vertical ionization. The results in Table V are obtained from the optimization of one molecule, while the second one was frozen (in case of dimers). It should be noted that this decision is straightforward for FDE in which the charge is localized on one subsystem; it does not enable a one-to-one comparison to supermolecular calculations as in these the charge might be distributed evenly over the subsystems.

In case of ethylene, the monomer value relaxes by about 0.24–10.03 eV. This rather small change indicates that the geometry is not significantly perturbed in this case after relaxation in the IP state. Similar to the purely vertical excitations, in case of the supermolecular calculations, the relative influence of the second molecule is reducing the IPs even further to 8.78 eV of which the relative shift to the relaxed monomer is similar to the vertical transition.

In case of pyrimide, the monomer value relaxes significantly by −1.15 eV to 7.56 eV, and accordingly, geometry changes can be

TABLE V. Ethylene and pyrimidine dimer geometry-relaxed ionization potentials in eV calculated with different methods as implemented in the KOALA program with and without embedding. Values in parentheses denote the shift with respect to the corresponding monomer in the corresponding method. In case of dimers, both the distance between two subsystems and the environment molecule geometry are kept frozen.

Molecule	System	Distance (Å)	IP-CIS(D_∞)	IP-ADC(2)
Ethylene dimer	Superm.	3.0	8.84 (−1.19)	8.84 (−1.19)
		5.0	9.92 (−0.11)	9.92 (−0.11)
		7.5	10.00 (−0.03)	10.00 (−0.03)
	FDE	3.0	9.78 (−0.25)	9.78 (−0.25)
		5.0	9.95 (−0.08)	9.95 (−0.08)
		7.5	10.01 (−0.02)	10.01 (−0.02)
	Monomer		10.03	10.03
Pyrimidine dimer	Superm.	3.0	7.22 (−0.34)	7.22 (−0.34)
		5.0	7.48 (−0.08)	7.48 (−0.08)
		7.5	7.53 (−0.03)	7.53 (−0.03)
	FDE	3.0	7.47 (−0.09)	7.47 (−0.09)
		5.0	7.52 (−0.04)	7.52 (−0.04)
		7.5	7.54 (−0.02)	7.54 (−0.02)
	Monomer		7.56	7.56

Published under license by AIP Publishing

TABLE VI. Azulene dimer vertical electron attachment energies in eV calculated with different methods as implemented in the KOALA program with and without embedding. Values in parentheses denote the shift with respect to the monomer in the corresponding method. The monomer EA obtained from CCSD with a numerical continuum orbital is −0.53 eV. The monomer EA obtained from ΔCCSD(T) is −0.47 eV, with a large spin contamination at the self-consistent field (SCF) level with $\langle S^2 \rangle_{SCF} = 1.253$. The experimental adiabatic electron attachment energy (AEA) for azulene is −0.8 ± 0.1 eV.[73,74]

System	Distance (Å)	EA-CIS(D_∞)	EA-ADC(2)	EA-CC2
Superm.	3.0	−1.42 (−0.41)	−1.42 (−0.41)	−1.31 (−0.43)
	5.0	−0.98 (+0.03)	−0.98 (+0.03)	−0.86 (+0.02)
	7.5	−0.97 (+0.04)	−0.97 (+0.04)	−0.84 (+0.04)
FDE	3.0	−0.78 (+0.23)	−0.79 (+0.22)	−0.66 (+0.22)
	5.0	−0.89 (+0.12)	−0.89 (+0.12)	−0.76 (+0.12)
	7.5	−0.95 (+0.06)	−0.95 (+0.06)	−0.88 (+0.00)
Monomer		−1.01	−1.01	−0.88

observed in the molecule. For example, the angle ∠(NCN) reduces from 127° to 113°, while the nitrogen–nitrogen distance reduces by about 0.2 Å from 2.39 Å to 2.21 Å. However, similar to ethylene and the purely vertical transitions, for pyrimidine, the dimer exhibits no strong interactions so that even in the supermolecular approach, the change in the IP is significantly less pronounced.

Finally, the active subsystems, at which the charge is localized, are optimized, while the environment is frozen using the FDE ansatz. Similar to the purely vertical transitions, the FDE ansatz reduces the interaction although the reduction goes even further for the relaxed systems. For example, in case of pyrimidine, the CIS(D_∞) vertical transition is reduced from −0.45 eV to −0.11 eV, while in case of the relaxed geometries, it is reduced from −0.34 eV to −0.09 eV.

C. Electron attachment energies

In order to investigate the accuracy of the present approach for electron attachment energies, in the present work, the azulene molecule is discussed, see Fig. 2, since the ethylene anion is not stable. Azulene is well characterized and has a stable anion, which is also experimentally confirmed. Results for this molecule are collected in Table VI, including monomer results, dimer results, see Fig. 1, and values obtained using the reference methods.

The target methods are in qualitative agreement with the experimental adiabatic electron attachment energy of −0.8 ± 0.1 eV.[73,74] The reference methods ΔCCSD(T) and CCSD yield a significantly smaller vertical transition energy of about −0.5 eV for the employed geometry, which might be rooted in comparing a computed vertical transition with a measured adiabatic transition. Altogether, the supermolecular calculations seem to differ strongly from the FDE results. For example, the dimer at 3.0 Å has a shift of about −0.4 in the supermolecular approach, while it is ∼+0.2 eV using FDE.

In order to analyze the azulene case more closely, we have computed atomic charges by fitting these to reproduce the electrostatic potential (ESP) of the orbital-relaxed EA-ADC(2) densities. Results are collected in Table VII. The atomic charges show that in case of the supermolecular dimer calculation, the charge is evenly distributed among the subsystems, while in case of FDE,

TABLE VII. Atomic charges in *e* from an ESP fit based on the orbital-relaxed EA-ADC(2) density (using a neutral reference) for an azulene monomer and dimer (at 3.0 Å). Vertical electron attachment energies are given in Table VI. The atom numbering is illustrated in Fig. 2.

	Monomer		Superm. MP2 [a]		MP2-in-MP2 [a]		Superm. EA-ADC(2)		EA-ADC(2)-in-MP2	
Atom	I	II	I	II	I	II	I	II	I	II
C_1	−0.43	−0.18[a]	−0.15	−0.14	−0.17	−0.17	−0.12	−0.11	−0.44	−0.18[a]
C_4	+0.40	+0.31[a]	+0.32	+0.32	+0.31	+0.31	+0.40	+0.39	+0.42	+0.32[a]
C_5	−0.64	−0.53[a]	−0.57	−0.57	−0.53	−0.53	−0.70	−0.69	−0.63	−0.53[a]
H_1	+0.11	+0.14[a]	+0.14	+0.14	+0.13	+0.13	+0.12	+0.12	+0.10	+0.13[a]
H_2	+0.03	+0.10[a]	+0.12	+0.12	+0.08	+0.08	+0.12	+0.13	+0.01	+0.08[a]
H_5	+0.20	+0.21[a]	+0.23	+0.23	+0.20	+0.20	+0.25	+0.25	+0.19	+0.20[a]
$\sum$[b]	−1.0	0.0	0.0	0.0	0.0	0.0	−0.5	−0.5	−1.0	0.0

[a] ESP charges obtained from orbital-relaxed MP2.
[b] The sum of the system's atomic charges.

Published under license by AIP Publishing

the charge is forced on one subsystem. This charge separation is clearly reflected in the atomic charges. For example, while in case of supermolecular EA-ADC(2), the charges are "symmetric" and significantly differ from both the charged and neutral monomer values; in case of EA-ADC(2) with FDE, the monomer charges are retained.

1. Geometry relaxation

Having assessed the accuracy of the methods for vertical electron attachment energy, we again turn to transitions for relaxed geometries, that is, the relaxation energy due to electron attachment. Results collected in Table VIII are obtained from the optimization of one molecule, while the second one was frozen (in case of dimers). Similar to the IP case, this strategy is straightforward for FDE in which the charge is localized on one subsystem, but it does not enable a one-to-one comparison to supermolecular calculations as in these the charge is distributed evenly over the subsystems, as discussed in the context of Table VII.

The transition energy of azulene is reduced by about −0.25 eV to −1.33 eV. In case of a neutral system, the supermolecular results show a strong interaction at 3.0 Å and they converge to the monomer results with increasing dimer distance. However, it can be seen that in the supermolecular calculations, the sign of the shift is also inverted for 5.0 Å and 7.5 Å. The reason might be rooted in a localization of the electron on one molecule. Using FDE, the interaction is reduced, and similar to the purely vertical transitions, the sign is inverted even for the close distance of 3.0 Å.

D. Tetraazaperopyrenes

In this section, we apply the new methods to tetraazaperopyrene (TAPP) derivatives to study their properties and in particular their change due to molecular environments. TAPP compounds can be tuned using two different substituents *X* and *R*; see Fig. 3. The substituents *R* have been shown to be important for the packing of the crystal structure but rather unimportant for excited states since the alkyl chains do not participate in the lowest excited state. The substituents *X* tune the properties of the valence electrons, in particular excited states and changes such as the absorption spectra.[82] In order to quantify the impact of the different substituents for IP and EA values, we, therefore, investigate the properties of all monomer compounds R-TAPP-X and the selected clusters of H-TAPP-H, cf. Fig. 4, in the following.

TABLE VIII. Azulene dimer geometry-relaxed electron attachment energies in eV calculated with different methods as implemented in the KOALA program with and without embedding. Values in parentheses denote the shift with respect to the corresponding monomer in the corresponding method. In case of dimers, both the distance between two subsystems and the environment molecule geometry are kept frozen.

Molecule	System	Distance (Å)	EA-CIS(D_∞)	EA-ADC(2)
Azulene	Superm.	3.0	−1.53 (−0.20)	−1.53 (−0.20)
		5.0	−1.28 (+0.05)	−1.28 (+0.05)
		7.5	−1.29 (+0.04)	−1.29 (+0.04)
	FDE	3.0	−1.11 (+0.22)	−1.11 (+0.22)
		5.0	−1.21 (+0.12)	−1.21 (+0.12)
		7.5	−1.27 (+0.06)	−1.27 (+0.06)
	Monomer		−1.33	−1.33

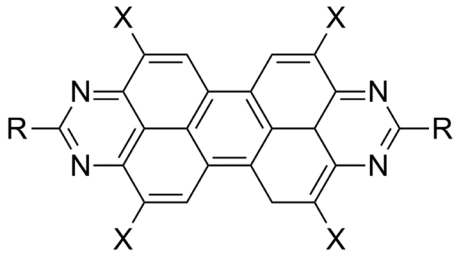


FIG. 3. Lewis representation of the R-TAPP-X molecules, where X = {H, F, Cl, Br} and R = {H, C_3F_7}.

1. Ionization potentials

Ionization potential results for different TAPP systems are collected in Table IX. First of all, it can be seen that the result of the present work is in good agreement with G_0W_0 calculations, agreeing within about 0.05 eV for almost all cases. One exception is the H-TAPP-H for which the G_0W_0 method shows a value which is shifted by about 0.1 eV. The PBE0 results, i.e., the HOMO energies, show rather large errors with deviations of about 1 eV to G_0W_0 and the wavefunction methods, revealing that orbital energies can only be used as a qualitative measure if they have to be used.

This table also shows the influence of the different substituents upon the IP. While the substituents *X* has no significant effect on the IP, the substituents *R* yield an almost constant shift of ~0.5 eV to higher IP values; cf. Ref. 6. In a single-particle picture, the substituents *R* can be understood to shift both the HOMO and the LUMO so that a significant shift for the IP (and EA) is obtained, while the lowest electronically excited states are not affected by different substituents *R*.

Table IX also contains values for increased models of TAPP crystals, namely, the dimer, trimer, and a cluster containing 21 H-TAPP-H molecules in total. For the dimer and trimer, the G_0W_0 method predicts a pronounced change in the IP, while the wavefunction methods, computed using FDE, yield a reduced dependence. This can, however, be related to the FDE approximation; cf. Table VII.

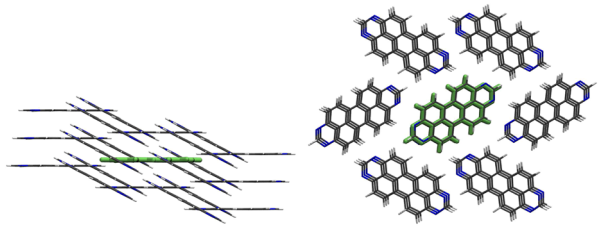


FIG. 4. Side view (left) and top view (right) of a cluster consisting of seven stacks containing three layers each resulting in 21 H-TAPP-H molecules (756 atoms) in total, as extracted from the experimental crystal structure.[80,81] The $\pi - \pi$ interplanar distance is 3.37 Å in the crystal.

Published under license by AIP Publishing

TABLE IX. R-TAPP-X vertical ionization potentials in eV.

Molecule	PBE0[a,b]	G_0W_0[b]	IP-CIS(D_∞)	IP-ADC(2)
H-TAPP-H	6.52	7.60	7.50	7.50
H-TAPP-F	6.64	7.73	7.68	7.68
H-TAPP-Cl	6.64	7.67	7.61	7.61
H-TAPP-Br	6.66	7.66	7.60	7.60
C_3F_7-TAPP-H	7.08	8.12	8.09	8.09
C_3F_7-TAPP-F	7.23	8.27	8.30	8.30
C_3F_7-TAPP-Cl	7.09	8.08	8.10	8.10
C_3F_7-TAPP-Br	7.08	8.06	8.07	8.07
H-TAPP-H dimer	6.47 (−0.05)	7.47 (−0.13)	7.48 (−0.02)[c]	7.48 (−0.02)[c]
H-TAPP-H trimer	6.46 (−0.06)	7.40 (−0.20)	7.47 (−0.03)[c]	7.47 (−0.03)[c]
H-TAPP-H cluster[d]	×[e]	×[e]	7.51 (+0.01)[c]	7.51 (+0.01)[c]

[a]Computed using TURBOMOLE.
[b]HOMO energy.
[c]FDE calculations with KOALA.
[d]The center molecule of the TAPP cluster with 21 molecules consisting of 756 atoms in total.
[e]Not computed.

2. Electron attachment energies

Results for electron attachments for different TAPP systems are collected in Table X. Similar to the IP case, it can be seen that the results of the present work are in good agreement with G_0W_0 calculations, agreeing with an almost constant shift of about 0.5 eV. The PBE0 results, i.e., the LUMO energies, show rather large errors with deviations of about 1 eV to G_0W_0 and the wavefunction methods, revealing that orbital energies can only be used as a qualitative measure if they can be used at all.

This table also shows the influence of the different substituents upon the EA. In contrast to IPs, now the substituents *X* have a pronounced effect on the EA, while the substituents *R* yield again an almost constant shift to higher EA values; cf. Ref. 6.

Table X also contains values for increased models of TAPP compounds, namely, the dimer, trimer, and a cluster containing

TABLE X. R-TAPP-X vertical electron attachment energy in eV. Values in parentheses are calculated with the SVPD basis set for the active subsystem and the SVP basis set for the environment subsystems in case of FDE, while the SVPD basis set was used for the whole system in case of supermolecular calculation.

Molecule	PBE0[a,b]	G_0W_0[a]	EA-CIS(D_∞)	EA-ADC(2)
H-TAPP-H	−3.27 (−3.31)	−2.09 (−1.80)	−2.36 (−2.14)	−2.36 (−2.15)
H-TAPP-F	−3.57	−2.40	−2.74	−2.74
H-TAPP-Cl	−3.70	−2.62	−3.03	−3.03
H-TAPP-Br	−3.73	−2.69	−3.14	−3.14
C_3F_7-TAPP-H	−3.82	−2.68	−2.98	−2.98
C_3F_7-TAPP-F	−4.16	−3.05	−3.42	−3.42
C_3F_7-TAPP-Cl	−4.16	−3.12	−3.56	−3.56
C_3F_7-TAPP-Br	−4.17	−3.17	−3.65	−3.65
H-TAPP-H dimer	−3.41 (−3.46)	−2.34 (−2.08)	−2.35 (−2.13)[c]	−2.35 (−2.13)[c]
H-TAPP-H trimer	×[d] (−3.21)[c]	×[d]	−2.33 (−2.11)[c]	−2.33 (−2.11)[c]
H-TAPP-H cluster[e]	×[d]	×[d]	×[d] (−2.17)[c]	×[d] (−2.18)[c]

[a]Computed with TURBOMOLE.
[b]LUMO energy.
[c]FDE calculation with KOALA.
[d]Not computed.
[e]The center molecule of the TAPP cluster with 21 molecules consisting of 756 atoms in total.

Published under license by AIP Publishing

TABLE XI. H-TAPP-H geometry-relaxed ionization and electron-attachment energies in eV. Values in parentheses denote the difference to the corresponding monomer and dimer values for IPs and EAs in Tables IX and X, respectively.

	IP		EA	
Molecule	IP-CIS(D_∞)	IP-ADC(2)	EA-CIS(D_∞)	EA-ADC(2)
Monomer	7.33 (−0.17)[a]	7.33 (−0.17)[a]	−2.74 (−0.38)[b]	−2.74 (−0.38)[b]
Dimer	7.31 (−0.17)[a]	7.31 (−0.17)[a]	−2.52 (−0.38)[c]	−2.52 (−0.37)[c]

[a]TZVP basis set.
[b]TZVPD basis set.
[c]SVPD basis set for an active subsystem and the SVP basis set for an environment subsystem.

21 H-TAPP-H molecules in total. For the dimer and trimer, the G_0W_0 method predicts a pronounced change in the EA compared to the wavefunction methods, computed with FDE, yielding a reduced dependence. This can, however, be related to the FDE approximation. For example, calculating a dimer as an active subsystem in a cluster consisting of 28 H-TAPP-H molecules using ADC(2) FDE yields an EA value of −2.54 eV, which corresponds to a shift of about −0.4 eV compared to the monomer value of −2.14 eV. This value of −0.4 eV can be related to the strong shift of about −0.28 eV in case of supermolecular G_0W_0, i.e., from −1.80 eV to −2.08 eV in the dimer without environment cluster contributions.

Finally, we have studied the effect of geometry relaxation for the H-TAPP-H compound after electron loss and attachment. Results are collected in Table XI. This table shows that the geometry relaxation yields an energy decrease of about −0.2 eV in case of IPs and a slightly more pronounced energy decrease of about −0.4 eV in case of EAs. However, the charges do not lead to significant changes in the molecular geometry, which is desirable for efficient organic semiconductors.[83]

IV. SUMMARY AND CONCLUSIONS

In the present work, we report the derivation and implementation to compute vertical ionization potentials (IPs) and electron affinities (EAs) for embedded wavefunction methods as well as the corresponding analytical nuclear gradients for IP/EA-ADC(2) as well as IP/EA-CIS(D_∞). The methods were applied to selected case studies, with an emphasis on localizing the charges as introduced by the EOM-IP and EOM-EA ansatz in dimers. For the selected dimers, the error of the dimer shift in the supermolecular calculations is computed to be below 0.5 eV compared to supermolecular reference CCSD results for the distance at 3 Å, while for increased distances of 5 Å and 7 Å, the deviation to reference methods is found to be sufficiently small. The embedding approach localizes the charge onto one molecule, which has some conceptual advantages for studying charge transfer in molecular crystals. Additionally, it reduces significantly the computational costs, allowing us to study the TAPP derivatives used as organic semiconductors in increased cluster models.

The FDE ansatz enforces a localization of the charge on one subsystem and can thus lead to significant differences with respect to supermolecular calculations, in particular for short distances. However, the FDE ansatz allows also to include, for example, two TAPP molecules in the active subsystem, see Sec. III D 2, allowing us to study long-range effects and also to investigate coupling in different directions.

The methods implemented in the present work are based on a previous implementation of analytical nuclear gradients for excited-state CC2 combined with FDE. While ADC(2) and CC2 are sufficiently accurate in most cases for purely valence-excited states, IP-ADC(2) and EA-ADC(2) can exhibit deviations in terms of absolute values of about 2 eV for IPs and EAs compared to IP-CCSD or EA-CCSD, respectively. Future work should address gradient contributions due to embedding potentials polarized by the electron change and corrections toward IP-CCSD$[k]_{CC2}$[79] or ADC(2)-x.[84]

ACKNOWLEDGMENTS

This work has been supported by the Deutsche Forschungsgemeinschaft (DFG) through No. SFB 1249, "*N*-Heteropolycycles as Functional Materials" (Project B07).

APPENDIX: OBTAINING WORKING EQUATIONS FOR THE JACOBIAN LEFT-HAND TRANSFORMATION

For a transformation of the Jacobian A_{μ^h,ν^h} from the left, one obtains in a doubles-direct formulation only a residual ρ for the singles, while the doubles are constructed on-the-fly,

$$\rho_x^i = -\sum_j E_{ji}\bar{L}_x^j - \sum_{dlk}(ld|ik)\bar{L}_{dx}^{kl}, \tag{A1}$$

$$\bar{L}_{ax}^{ij} = \frac{2(ia\breve{|}jx) - (ix\breve{|}ja) + P_{ij}^{ax}(2\bar{L}_a^i F_{jx} - \bar{L}_x^i F_{ja})}{\varepsilon_x + \varepsilon_a - \varepsilon_i - \varepsilon_j}. \tag{A2}$$

The breve accent indicates that the integral has to be computed in the following manner:

$$(pq\breve{|}rs) = P_{pr}^{qs}[(\breve{p}^p q^h|r^p s^h) + (p^p \breve{q}^h|r^p s^h)] \tag{A3}$$

$$= [(\breve{p}^p q^h|r^p s^h) + (p^p \breve{q}^h|r^p s^h)] + [(\breve{r}^p s^h|p^p q^h) + (r^p \breve{s}^h|p^p q^h)]. \tag{A4}$$

Working out the equations yields the following non-vanishing contributions:

$$(ia\breve{|}jx) = (j^p \breve{x}^h|i^p a^h) = -\sum_k \bar{L}_x^k (j^p k^h|i^p a^h), \tag{A5}$$

$$(ix\breve{|}ja) = (i^p \breve{x}^h|j^p a^h) = -\sum_k \bar{L}_x^k (i^p k^h|j^p a^h). \tag{A6}$$

Published under license by AIP Publishing

REFERENCES

[1] S. E. Shaheen, D. S. Ginley, and G. E. Jabbour, MRS Bull. **30**, 10–19 (2005).
[2] G. Inzelt, M. Pineri, J. W. Schultze, and M. A. Vorotyntsev, Electrochim. Acta **45**, 2403 (2000).
[3] C. Wang, H. Dong, L. Jiang, and W. Hu, Chem. Soc. Rev. **47**, 422 (2018).
[4] J. D. Myers and J. Xue, Polym. Rev. **52**, 1 (2012).
[5] V. Coropceanu, J. Cornil, D. A. da Silva Filho, Y. Olivier, R. Silbey, and J.-L. Brédas, Chem. Rev. **107**, 926 (2007).
[6] L. Hahn, F. Maaß, T. Bleith, U. Zschieschang, H. Wadepohl, H. Klauk, P. Tegeder, and L. H. Gade, Chem. Eur. J. **21**, 17691 (2015).
[7] S. C. Martens, U. Zschieschang, H. Wadepohl, H. Klauk, and L. H. Gade, Chem. Eur. J. **18**, 3498 (2012).
[8] T. Riehm, G. De Paoli, A. E. Konradsson, L. De Cola, H. Wadepohl, and L. H. Gade, Chem. Eur. J. **13**, 7317 (2007).
[9] L. Hahn, A. Hermannsdorfer, B. Günther, T. Wesp, B. Bühler, U. Zschieschang, H. Wadepohl, H. Klauk, and L. H. Gade, J. Org. Chem. **82**, 12492 (2017).
[10] J. L. Bredas, J. P. Calbert, D. A. da Silva Filho, and J. Cornil, Proc. Natl. Acad. Sci. U. S. A. **99**, 5804 (2002).
[11] P. Mori-Sánchez, A. J. Cohen, and W. Yang, Phys. Rev. Lett. **100**, 146401 (2008).
[12] A. Seidl, A. Görling, P. Vogl, J. A. Majewski, and M. Levy, Phys. Rev. B **53**, 3764 (1996).
[13] M. K. Y. Chan and G. Ceder, Phys. Rev. Lett. **105**, 196403 (2010).
[14] L. Hedin, Phys. Rev. **139**, A796 (1965).
[15] F. Aryasetiawan and O. Gunnarsson, Rep. Prog. Phys. **61**, 237 (1998).
[16] H. Lambert and F. Giustino, Phys. Rev. B **88**, 075117 (2013).
[17] T. Kotani, M. van Schilfgaarde, and S. V. Faleev, Phys. Rev. B **76**, 165106 (2007).
[18] M. van Schilfgaarde, T. Kotani, and S. Faleev, Phys. Rev. Lett. **96**, 226402 (2006).
[19] N. Marom, F. Caruso, X. Ren, O. T. Hofmann, T. Körzdörfer, J. R. Chelikowsky, A. Rubio, M. Scheffler, and P. Rinke, Phys. Rev. B **86**, 245127 (2012).
[20] X.-Z. Li, R. Gómez-Abal, H. Jiang, C. Ambrosch-Draxl, and M. Scheffler, New J. Phys. **14**, 023006 (2012).
[21] D. Danovich, WIREs Comput. Mol. Sci. **1**, 377 (2011).
[22] M. J. van Setten, F. Weigend, and F. Evers, J. Chem. Theory Comput. **9**, 232 (2013).
[23] I.-H. Chu, J. P. Trinastic, Y.-P. Wang, A. G. Eguiluz, A. Kozhevnikov, T. C. Schulthess, and H.-P. Cheng, Phys. Rev. B **93**, 125210 (2016).
[24] F. Bruneval and X. Gonze, Phys. Rev. B **78**, 085125 (2008).
[25] H.-V. Nguyen, T. A. Pham, D. Rocca, and G. Galli, Phys. Rev. B **85**, 081101 (2012).
[26] T. A. Pham, H.-V. Nguyen, D. Rocca, and G. Galli, Phys. Rev. B **87**, 155148 (2013).
[27] T. Körzdörfer and N. Marom, Phys. Rev. B **86**, 041110 (2012).
[28] V. Atalla, M. Yoon, F. Caruso, P. Rinke, and M. Scheffler, Phys. Rev. B **88**, 165122 (2013).
[29] J. Schirmer, Phys. Rev. A **26**, 2395 (1982).
[30] J. F. Stanton and R. J. Bartlett, J. Chem. Phys. **98**, 7029 (1993).
[31] J. Geertsen, M. Rittby, and R. J. Bartlett, Chem. Phys. Lett. **164**, 57 (1989).
[32] O. Christiansen, P. Jørgensen, and C. Hättig, Int. J. Quantum Chem. **68**, 1 (1998).
[33] A. Dreuw and M. Wormit, Wiley Interdiscip. Rev.: Comput. Mol. Sci. **5**, 82 (2015).
[34] J. H. Starcke, M. Wormit, and A. Dreuw, J. Chem. Phys. **130**, 024104 (2009).
[35] O. Christiansen, H. Koch, and P. Jørgensen, Chem. Phys. Lett. **243**, 409 (1995).
[36] A. Köhn and C. Hättig, J. Chem. Phys. **119**, 5021 (2003).
[37] A. Pershin and P. G. Szalay, J. Chem. Theory Comput. **11**, 5705 (2015).
[38] M. Head-Gordon, M. Oumi, and D. Maurice, Mol. Phys. **96**, 593 (1999).
[39] N. O. C. Winter, N. K. Graf, S. Leutwyler, and C. Hättig, Phys. Chem. Chem. Phys. **15**, 6623 (2013).
[40] C. Hättig, Adv. Quantum Chem. **50**, 37 (2005).
[41] R. Send, M. Kühn, and F. Furche, J. Chem. Theory Comput. **7**, 2376 (2011).
[42] R. O. Jones and O. Gunnarsson, Rev. Mod. Phys. **61**, 689 (1989).
[43] O. Gunnarsson and B. I. Lundqvist, Phys. Rev. B **13**, 4274 (1976).
[44] A. Shee, T. Saue, L. Visscher, and A. Severo Pereira Gomes, J. Chem. Phys. **149**, 174113 (2018).
[45] S. Hirata, M. Nooijen, and R. J. Bartlett, Chem. Phys. Lett. **328**, 459 (2000).
[46] M. Nooijen and R. J. Bartlett, J. Chem. Phys. **102**, 3629 (1995).
[47] M. Musiał, S. A. Kucharski, and R. J. Bartlett, J. Chem. Phys. **118**, 1128 (2003).
[48] J. F. Stanton and J. Gauss, J. Chem. Phys. **101**, 8938 (1994).
[49] T. A. Wesolowski and A. Warshel, J. Phys. Chem. **97**, 8050 (1993).
[50] A. Severo Pereira Gomes and C. R. Jacob, Annu. Rep. Prog. Chem., Sect. C: Phys. Chem. **108**, 222 (2012).
[51] C. R. Jacob and J. Neugebauer, Wiley Interdiscip. Rev.: Comput. Mol. Sci. **4**, 325 (2014).
[52] T. A. Wesolowski, S. Shedge, X. Zhou Chem. Rev. **115**, 5891 (2015).
[53] Y. Bouchafra, A. Shee, F. Réal, V. Vallet, and A. Severo Pereira Gomes, Phys. Rev. Lett. **121**, 266001 (2018).
[54] T. A. Barnes, J. W. Kaminski, O. Borodin, and T. F. Miller III, J. Phys. Chem. C **119**, 3865 (2015).
[55] S. J. Bennie, B. F. E. Curchod, F. R. Manby, and D. R. Glowacki, J. Phys. Chem. Lett. **8**, 5559 (2017).
[56] X. Wen, D. S. Graham, D. V. Chulhai, and J. D. Goodpaster, J. Chem. Theory Comput. **16**, 385 (2020).
[57] C. Hättig and F. Weigend, J. Chem. Phys. **113**, 5154 (2000).
[58] O. Vahtras, J. Almlöf, and M. W. Feyereisen, Chem. Phys. Lett. **213**, 514 (1993).
[59] K. Eichkorn, O. Treutler, H. Öhm, M. Häser, and R. Ahlrichs, Chem. Phys. Lett. **240**, 283 (1995).
[60] C. Hättig, J. Chem. Phys. **118**, 7751 (2003).
[61] J. F. Stanton and J. Gauss, J. Chem. Phys. **111**, 8785 (1999).
[62] N. K. Graf, D. H. Friese, N. O. C. Winter, and C. Hättig, J. Chem. Phys. **143**, 244108 (2015).
[63] C. Hättig and A. Köhn, J. Chem. Phys. **117**, 6939 (2002).
[64] A. S. P. Gomes, C. R. Jacob, and L. Visscher, Phys. Chem. Chem. Phys. **10**, 5353 (2008).
[65] J. Heuser and S. Höfener, J. Comput. Chem. **37**, 1092 (2016).
[66] J. Heuser and S. Höfener, J. Comput. Chem. **38**, 2316 (2017).
[67] KOALA, an *ab initio* electronic structure program, written by S. Höfener, with contributions from A.-S. Hehn, J. Heuser, and N. Schieschke.
[68] S. Höfener, J. Comput. Chem. **35**, 1716 (2014).
[69] J. P. Perdew, K. Burke, and M. Ernzerhof, Phys. Rev. Lett. **77**, 3865 (1996).
[70] A. Lembarki and H. Chermette, Phys. Rev. A **50**, 5328 (1994).
[71] F. Weigend, M. Häser, H. Patzelt, and R. Ahlrichs, Chem. Phys. Lett. **294**, 143 (1998).
[72] D. Rappoport and F. Furche, J. Chem. Phys. **133**, 134105 (2010).
[73] J. Schiedt, W. J. Knott, K. Le Barbu, E. W. Schlag, and R. Weinkauf, J. Chem. Phys. **113**, 9470 (2000).
[74] N. Ando, M. Mitsui, and A. Nakajima, J. Chem. Phys. **128**, 154318 (2008).
[75] F. Furche, R. Ahlrichs, C. Hättig, W. Klopper, M. Sierka, and F. Weigend, Wiley Interdiscip. Rev.: Comput. Mol. Sci. **4**, 91 (2014).
[76] TURBOMOLE V7.3 2018, A Development of University of Karlsruhe and Forschungszentrum Karlsruhe GmbH, 1989–2007, Turbomole GmbH, since 2007; available from http://www.turbomole.com.
[77] CFOUR, a quantum chemical program package written by J. F. Stanton, J. Gauss, L. Cheng, M. E. Harding, D. A. Matthews, P. G. Szalay with contributions from A. A. Auer, R. J. Bartlett, U. Benedikt, C. Berger, D. E. Bernholdt, Y. J. Bomble, O. Christiansen, F. Engel, R. Faber, M. Heckert, O. Heun, C. Huber, T.-C. Jagau, D. Jonsson, J. Jusélius, K. Klein, W. J. Lauderdale, F. Lipparini, T. Metzroth, L. A. Mück, D. P. O'Neill, D. R. Price, E. Prochnow, C. Puzzarini, K. Ruud, F. Schiffmann, W. Schwalbach, C. Simmons, S. Stopkowicz, A. Tajti, J. Vázquez, F. Wang, J. D. Watts and the integral packages MOLECULE (J. Almlöf and P. R. Taylor), PROPS (P. R. Taylor), ABACUS (T. Helgaker, H. J. Aa. Jensen, P. Jørgensen, and J. Olsen), and ECP routines by A. V. Mitin and C. van Wüllen, for the current version, see http://www.cfour.de.

Published under license by AIP Publishing

[78] C. G. Ning, K. Liu, Z. H. Luo, S. F. Zhang, and J. K. Deng, Chem. Phys. Lett. **476**, 157 (2009).
[79] G. Wälz, D. Usvyat, T. Korona, and M. Schütz, J. Chem. Phys. **144**, 084117 (2016).
[80] M. Matena, M. Stöhr, T. Riehm, J. Björk, S. Martens, M. S. Dyer, M. Persson, J. Lobo-Checa, K. Müller, M. Enache, H. Wadepohl, J. Zegenhagen, T. A. Jung, and L. H. Gade, Chem. Eur. J. **16**, 2079 (2010).
[81] M. Matena, M. Stöhr, T. Riehm, J. Björk, S. Martens, M. Dyer, M. Persson, J. Lobo-Checa, K. Müller, M. Enache, H. Wadepohl, J. Zegenhagen, T. Jung, and L. Gade, "Experimental crystal structure determination," CDCC 747374 (2010).
[82] S. Höfener, B. A. R. Günther, M. E. Harding, and L. H. Gade, J. Phys. Chem. A **123**, 3160 (2019).
[83] B. C. Lin, C. P. Cheng, and Z. P. M. Lao, J. Phys. Chem. A **107**, 5241 (2003).
[84] A. B. Trofimov and J. Schirmer, J. Phys. B: At., Mol. Opt. Phys. **28**, 2299 (1995).

Published under license by AIP Publishing